5-2021

A Modeling Study of the Mobilization and Sequestration of Trace Metals in a Crude-Oil-Contaminated Aquifer

Zoe M. Lacey

Trinity University, zoelacey99@gmail.com

Recommended Citation

Lacey, Zoe M., "A Modeling Study of the Mobilization and Sequestration of Trace Metals in a Crude-Oil-Contaminated Aquifer" (2021). *Geosciences Student Honors Theses*. 22.
https://digitalcommons.trinity.edu/geo_honors/22

A MODELING STUDY OF THE MOBILIZATION AND SEQUESTRATION OF TRACE METALS IN A CRUDE-OIL- CONTAMINATED AQUIFER

ZOE M. LACEY

A DEPARTMENT HONORS THESIS SUBMITTED TO THE
DEPARTMENT OF GEOSCIENCES AT TRINITY UNIVERSITY
IN PARTIAL FULFILLMENT OF THE REQUIREMENTS FOR GRADUATION WITH
DEPARTMENTAL HONORS

APRIL 23, 2020

BRADY A. ZIEGLER THESIS ADVISOR	KATHLEEN D. SURPLESS DEPARTMENT CHAIR

Michael Soto, AVPAA

Student Agreement

I grant Trinity University ("Institution"), my academic department ("Department"), and the Texas Digital Library ("TDL") the non-exclusive rights to copy, display, perform, distribute and publish the content I submit to this repository (hereafter called "Work") and to make the Work available in any format in perpetuity as part of a TDL, digital preservation program, Institution or Department repository communication, distribution or preservation effort.

I understand that once the Work is submitted, a bibliographic citation to the Work can remain visible in perpetuity, even if the Work is updated or removed.

I understand that the Work's copyright owner(s) will continue to own copyright outside these non-exclusive granted rights.

I warrant that:

1) I am the copyright owner of the Work, or
2) I am one of the copyright owners and have permission from the other owners to submit the Work, or
3) My Institution or Department is the copyright owner and I have permission to submit the Work, or
4) Another party is the copyright owner and I have permission to submit the Work.

Based on this, I further warrant to my knowledge:

1) The Work does not infringe any copyright, patent, or trade secrets of any third party,
2) The Work does not contain any libelous matter, nor invade the privacy of any person or third party, and
3) That no right in the Work has been sold, mortgaged, or otherwise disposed of, and is free from all claims.

I agree to hold TDL, Institution, Department, and their agents harmless for any liability arising from any breach of the above warranties or any claim of intellectual property infringement arising from the exercise of these non-exclusive granted rights.

I choose the following option for sharing my thesis (required):

[X] Open Access (full-text discoverable via search engines)
[ ] Restricted to campus viewing only (allow access only on the Trinity University campus via digitalcommons.trinity.edu)

I choose to append the following Creative Commons license (optional):

Abstract

Using a reactive transport model, I simulated the mobilization and sequestration of geogenic trace metals, nickel (Ni^{2+}) and cobalt (Co^{2+}), in a crude-oil-contaminated aquifer. These trace metals can pose threats to human and ecological health and are not commonly regulated or measured at oil-spill sites, making it important to characterize the geochemical mechanisms that release and attenuate potentially toxic trace metals. In the groundwater-contaminant plume, crude-oil is biodegraded coupled to iron (Fe(III)) reduction and methanogenesis. Previously collected field data[1] showed concentrations of Ni^{2+}, and Co^{2+} near the crude-oil source were elevated in groundwater and depleted from aquifer sediments compared to background concentrations. Roughly 80 meters downgradient, in the active Fe(III)-reducing zone, groundwater concentrations of Ni^{2+} and Co^{2+} decrease, relative to near the crude-oil body, and concentrations in sediment increase above background levels. Using a reactive transport model, I show that Ni^{2+} and Co^{2+} originally sorbed to Fe(III) are released from sediments near the oil body due to microbially mediated Fe(III)-reduction to aqueous Fe^{2+}. Biodegradation in the active Fe(III)-reducing zone, dissolves Fe^{2+} and produces bicarbonate, causing groundwater supersaturation with respect to siderite ($FeCO_3$), allowing $FeCO_3$ to precipitate. I developed a surface complexation model for Ni^{2+} and Co^{2+} on $FeCO_3$, to incorporate into our reactive transport model framework. Our modeling results showed that $FeCO_3$ generates negative surface charge in the pH range measured in the contaminant plume (6.3-7.3), allowing $FeCO_3$ to sorb Ni^{2+} and Co^{2+} and remove them from groundwater. Our modeling results were consistent with field observations. Previous sampling has shown that arsenic (As), which also is mobilized due to Fe(III) reduction, does not accumulate in Fe-reducing sediments like Ni^{2+} and Co^{2+}. The negative surface charge on $FeCO_3$ favors sorption of cations (Ni^{2+} and Co^{2+}) but not the (oxy)anions of As. Our model effectively delineated mechanisms that could release and attenuate trace metals at oil-spill sites, which can aid in more comprehensive predictions of threats to human and ecological health in aquifers contaminated by crude-oil.

1. Introduction

1.1 Background

Geogenic trace elements that originate in the aquifer solids are the most common type of groundwater contaminant[2]. Trace elements can contaminate groundwater through multiple mechanisms including reductive dissolution[3–5], acid-base-promoted desorption[6,7], sulfide oxidation[8–10], and geothermal activity[11,12], among others[13]. A common mechanism for trace element release is reductive dissolution of ferric iron (Fe(III))-containing minerals with trace elements sorbed to them. In the presence of organic matter in anoxic groundwater, organic carbon can be biodegraded (i.e., oxidized) coupled with the reduction of Fe(III) in the mineral to Fe(II), which is soluble in groundwater as the Fe^{2+} ion[14–16]. This mechanism has been observed in sewage[17], landfill[18], crude-oil[14–16], and petroleum/ethanol[19] contaminant plumes, and can occur with natural organic matter, resulting in widespread trace element contamination of groundwater, that can have implications for both environmental and human health[13,20,21].

Recent studies of a crude-oil-contaminated aquifer undergoing natural attenuation have documented numerous secondary water quality impacts, including plumes of various mobilized trace elements. For example, arsenic (As)[14–16] sorbed to Fe(III) hydroxides has been mobilized into groundwater where biodegradation is coupled with Fe(III)-reduction[13,14]. Follow-up field studies of the crude-oil-contaminated aquifer have found additional trace element plumes of nickel (Ni^{2+}), cobalt (Co^{2+}), strontium (Sr^{2+}), barium (Ba^{2+}), and chromium (Cr) [1,19].

Despite this aquifer being intensively studied over the past 35+ years, the phenomenon of trace element mobilization was only discovered in the past several years. While crude-oil chemicals pose their own water quality impairments, the mobilization of trace elements introduces additional water quality impairments with unique implications for human and environmental health. Some of these trace elements are regulated at the national level by the United States Environmental Protection Agency (EPA) (e.g., As) or recommended for regulation by the World Health Organization (WHO) (e.g., barium (Ba^{2+}) and nickel (Ni^{2+})) because of their link to adverse health outcomes. Toxic outcomes of barium exposure include cardiac and renal failure, and gastrointestinal problems[20]. Toxic outcomes of Ni^{2+} exposure include possible skin irritation[21]. Arsenic has been linked to multiple types of cancer [20–22]. Cobalt (Co^{2+}) is not currently regulated by the EPA but is under consideration through the EPA Contaminant Candidate List due to possible public health concerns related to its presence in public water supply[23].The negative health effects associated with these trace elements warrant more studies on the behavior of these geogenic elements in groundwater once mobilized.

This study uses a reactive transport model to elucidate mechanisms of trace element mobilization and sequestration in a crude-oil-contaminated aquifer near Bemidji, Minnesota. Natural attenuation, primarily driven by biodegradation, has altered the geochemistry of this aquifer[24] and introduced geogenic Ni^{2+} and Co^{2+} into groundwater of the contaminant plume. The goal in modeling the fate and transport of Ni^{2+} and Co^{2+} is to explore the related geochemical processes that can alter aquifer geochemistry. Changes to aquifer geochemistry can have adverse effects on environmental and human health making it pertinent to better understand mechanisms that are able to alter water quality.

1.2 Study Site

The aquifer at the Bemidji crude-oil contaminant site is a glacial outwash aquifer located within the Pleistocene Bagley Outwash Plain which consists primarily of a pitted sand and gravel outwash[25]. The aquifer is unconfined; the contaminated portion of the aquifer consists of moderately calcareous silty sand overlying clayey till with interbedded discontinuous silt layers interbedded with sand[25]. The sand fraction of sediment is approximately 60% quartz, 5% carbonates, 30% feldspars, and 5% heavy minerals; the silt fraction has a higher abundance of carbonate when compared to the bulk sediment[25]. Groundwater velocities were determined to range from 0.15 to 0.5 meters per day using the point dilution method for Darcy velocity [25].

In 1979 a crude oil pipeline ruptured, releasing 10,700 barrels of oil onto the land surface near Bemidji, Minnesota. Of the total oil spilled, ~2600 barrels percolated through the unsaturated zone and accumulated on the water table [26]. The oil body sitting on the water table acts as a source of dissolved organic carbon as the soluble and partially soluble crude-oil constituents from the oil body dissolve into groundwater to form a hydrocarbon contaminant plume. The plume stimulates microbial activity, that result in depleted dissolved oxygen due to aerobic respiration. This creates anoxic conditions, in which hydrocarbon biodegradation is then coupled to anaerobic terminal electron accepting processes (TEAPs)[14]. Fe(III)-reduction and methanogenesis are the primary TEAPS that facilitate biodegradation in the crude-oil plume[14]. The various TEAPs seen in the aquifer result in four distinct geochemical zones: the methanogenic zone near the crude-oil body, the anoxic Fe-reducing zone, the suboxic transition zone at the leading edge of the contaminant plume and on the plume fringes, and the uncontaminated, oxic background waters (Figure 1B)[14]. Since 1983, the Bemidji oil spill site has been a national research site through the U.S. Geological Survey (USGS) Toxic Substances Hydrology Program to study long-term natural attenuation of oil spills. Since then, decades of research have focused on this crude-oil contaminated aquifer to study the hydrogeology and biogeochemical processes which affect the aquifer. See Essaid et al.[27] for a summary of previous work[24,25,27–29].

Previous field studies have shown that groundwater in the crude-oil plume has elevated concentrations of Ni^{2+}, Co^{2+}, and As, among other trace elements. Each element has its own individual “plume”, the spatial extent~~s~~ of which is controlled by unique biogeochemical processes in the aquifer[1,14]. For example, an As plume extends from the oil body to roughly 130 m downgradient from well 421, this well is the reference datum demarcating the approximate center of the crude-oil body floating on the water table. Around 130 m, As is attenuated by sorbing to Fe-hydroxides in sediment, effectively remediating the As plume. Plumes of Ni^{2+} and Co^{2+}, in contrast, are attenuated by accumulating in sediment closer to the oil body, around 40 m downgradient from well 421. The difference in attenuation patterns between As and Co^{2+}/Ni^{2+} suggest that transport of these different trace elements is controlled by different geochemical processes.

A) Bemidji Site Map

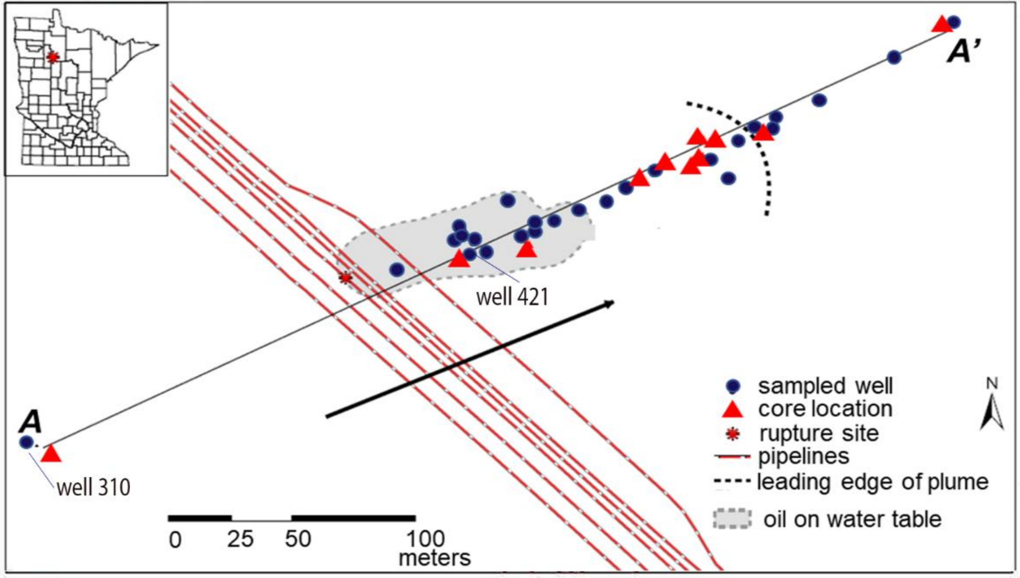

B) Conceptual Aquifer Zones

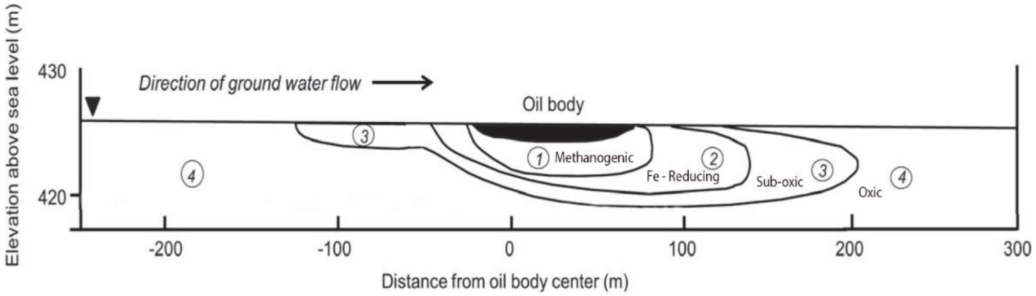

Figure 1. A) Map of the Bemidji contaminated aquifer along the center-line transect (A-A') of the oil plume adapted from Jones[1]. The map shows wells and sediment core locations where field data were collected and reported elsewhere[1,15,16,30], the rupture site, the pipelines, the leading edge of the plume, and crude oil floating on the water table. The inset shows the location of the spill within Minnesota. B) Conceptual diagram of geochemical zones in the aquifer, adapted from Cozzarelli et al.[14]. Zone 1 is methanogenic, zone 2 is Fe-reducing, zone 3 is sub-oxic, and zone 4 is oxic.

2. Methods

In this study, I expand upon a reactive transport model previously developed by Ng et al.[29] which took a comprehensive approach to modeling the processes occurring in the Bemidji aquifer known at the time of its development. The model incorporates biodegradation of organics coupled to multiple TEAPs[24,31–35],direct outgassing of CH_4 and CO_2, dissolution of CO_2, and sorption of reduced Fe^{2+} [29]. Later, the model was expanded upon to include new information about As cycling in the aquifer[15]. Now, I further expand upon this robust model to reflect new data about trace element cation cycling in the aquifer initially described by Jones[1]. The model now includes an expanded surface complexation model to describe Ni^{2+} and Co^{2+} sorption and desorption with respect to two sorbent phases, siderite ($FeCO_3$) and the Fe(III) hydroxide $Fe(OH)_3$, in an attempt to simulate the geochemical mechanism(s) responsible for mobilization and attenuation of geogenic trace elements in the contaminant plume. The model used PHT3D[36], which combines geochemical reactions from PHREEQC-2[37], groundwater flow from MODFLOW-2005[38], and solute transport from MT3DMS[39] (Figure 2).

2.1 Model domain and hydrogeologic parameters

A conceptual diagram of the model is shown in Figure 2. The original hydrogeologic parameters and model domain from the Ng et al.[29] model were used in this model. The simulation began with the oil-spill occurring in August 1979 and covered 15,000 days (through September 2020) (Figure 2). The model analysis domain depicts a two-dimensional cross-section of the groundwater plume, with each cell in the computational grid having dimensions of 4.3 m horizontally by 0.47 m vertically. The domain extends horizontally from 45 m upgradient to 215 m downgradient from the center of the oil body and vertically from 417 to 424 m above mean sea level. The computational grid extends to 475 m downgradient from the oil body and an elevation of 410 m to avoid boundary effects during model simulations. The upper boundary of the model domain is the water table.

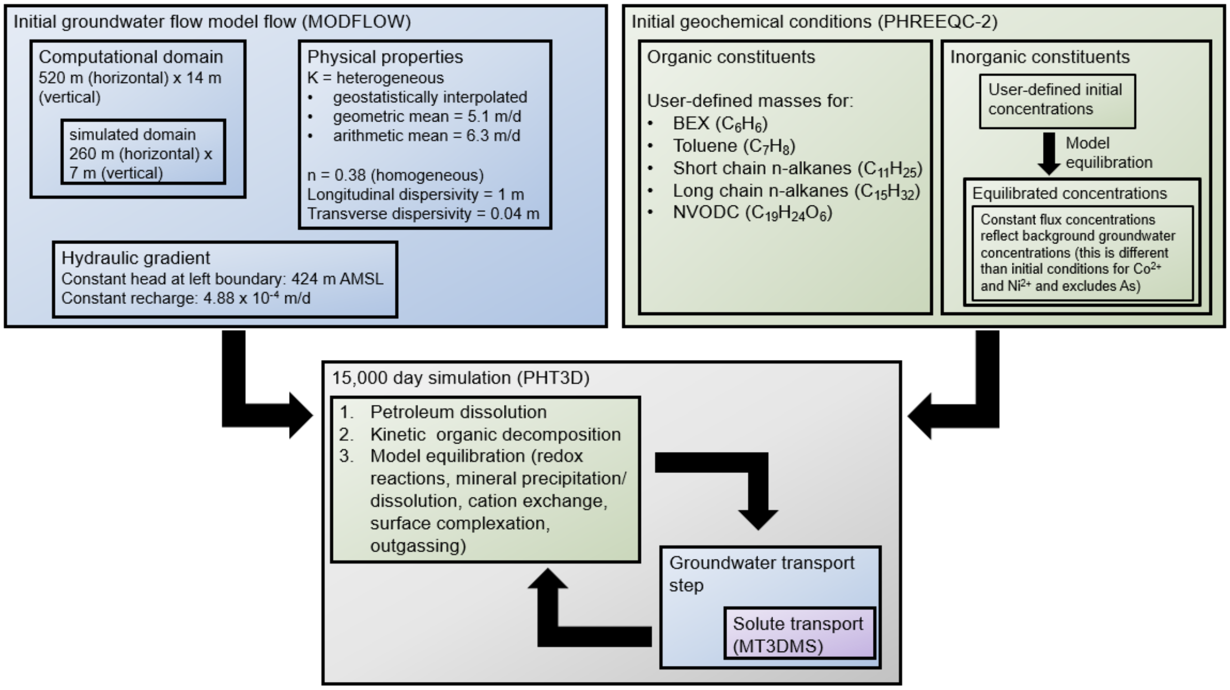

Figure 2. Model Conceptual Diagram. The top left blue box illustrates the components of the initial groundwater flow model (MODFLOW-2005). The top right green box illustrates components of the initial geochemical conditions (PHREEQC-2). The bottom grey box illustrates the simulation steps performed by PHT3D that incorporate both geochemical reactions performed by PHREEQC-2, groundwater transport performed by MODFLOW-2005, and solute transport performed by MT3DMS.

A porosity of 0.38 was chosen based on grain size analyses reported in Dillard et al.[40] and assigned homogeneously to the model due to the low variability (± 0.04) amongst the 269 samples. Hydraulic conductivity (K) in the aquifer was determined based on 58 slug tests performed in different wells in the aquifer. Slug test results showed that K ranged from 10^{-3} to 10 m/d with a median of 6.3 m/d [41]. K was applied heterogeneously to the model with geometric (5.1 m/d) and arithmetic (6.3 m/d) means based on geostatistical interpolations of the grain size analyses from sediment collected from the study site[40] and then inflated for a closer match to the homogeneous 6.1 m/d determined by Essaid et al.[32] (Figure 2).Longitudinal (1 m) and transverse (0.04 m) dispersivities based on a field tracer test, were applied uniformly to the model domain[32]. To produce the observed average hydraulic gradient (0.0035), a steady state flow field was imposed by applying a constant head boundary of 424 m above sea level at the left boundary with a constant recharge rate of 4.88×10^{-4} m/d (Figure 2) as determined by inverse modeling[32]. Partial oil saturation is achieved through a relative water permeability while the oil phase is modeled as stationary in time.

2.2 Geochemical formulation

Modeled aqueous inorganic species include inorganic C, CH_4, dissolved oxygen (DO), Mn, Fe, Ca, Cl, Na, H, inert N, As(III), As(V), Co, and Ni. Pyrolusite (MnO_2), amorphous ferric hydroxide ($Fe(OH)_3$), rhodochrosite ($MnCO_3$), and siderite ($FeCO_3$) are allowed to precipitate because they act as mineral sinks for elevated Fe^{2+} and Mn^{2+} in groundwater due to biodegradation. Calcite is included due to its role in carbonate chemistry. Species sorbed via cation exchange (HX, FeX_2 and MnX_2) and surface complexes for Co^{2+}, Ni^{2+}, As(V) (arsenate), As(III) (arsenite), and HCO_3^- are included in the model. Dissolved gas phases (CO_2, CH_4, O_2, and inert N_2) are used to simulate outgassing. For equilibrium reactions, with the exception of $Fe(OH)_3$ and $FeCO_3$, logK values from the default PHREEQC database were used. Values of equilibrium constants for $Fe(OH)_3$ and $FeCO_3$ dissolution and cation exchange were calibrated by Ng et al.[29].

Organic carbon degradation is modeled for four oil constituents: BEX (benzene, ethylbenzene, and xylenes, all modeled as one component), toluene, long- and short-chain *n*-alkanes, and oil constituents contributing to non-volatile dissolved organic carbon (NVDOC) (Figure 2). The degradation processes were determined based on dissolution pathways, biodegradation pathways, and oil loss pathways described in detail by Ng et al.[28]. Briefly, the dissolution and biodegradation rate parameters were calibrated based on field data from 1979[28,29,32,42–45], 1987 ±2[24,25,42], 1993 ±2[28,45,46], and 2008 ±2[28,42,43,47–52]. Unique dissolution rates and first-order biodegradation rates under different TEAPs were assigned to each constituent. BEX is assumed to follow a multicomponent dissolution rate while *n*-alkane oxidation has kinetic rates set explicitly for methanogenic biodegradation.

A partial equilibrium approach[53] was used for the geochemical model. This approach assumes that the organic carbon oxidation step is the rate-limiting step, and the associated reduction step proceeds as an equilibrium reaction. This is accomplished using PHT3D by irreversibly breaking down an organic molecule at a specific rate into its constitutive elements and valence states. The reactions and first-order rate constants for the oxidation of the four organic constituents are reported in Table 1.

Table 1. Kinetic biodegradation reactions and first-order rate coefficients

Kinetic reactions	First-order rate coefficient (s^{-1})
BEX	
$C_6H_6 \rightarrow 6C(-1) + 6H(+1)$	1.00×10^{-8}
Toluene	
$C_7H_8 \rightarrow 7C(-1) + 8H(+1)$	3.50×10^{-9}
NVDOC	
$C_{19}H_{24}O_6 \rightarrow 19C(-1) + 24H(+1) + 6O(-2)$	1.47×10^{-8}
short chain n-alkanes	
$C_{11}H_{25} \rightarrow 11C(-1) + 25H(+1)$	7.60×10^{-10}
long chain n-alkanes	
$C_{15}H_{32} \rightarrow 15C(-1) + 32H(+1)$	1.10×10^{-9}

The constitutive elements are then reintroduced into the equilibrium model, where C(-1) is then converted to the inorganic carbon form (i.e., HCO_3^-) via the most thermodynamically favorable TEAP based on the model chemistry (Table 2). Note that coefficients a, b, and c in Table 2 are determined by the kinetic oxidation of hydrocarbons (Table 1), and the consequent stoichiometry is then necessarily dependent upon coefficients a, b, and c for a given reaction. Reactions proceed sequentially from aerobic respiration to manganese reduction, followed by iron reduction and methanogenesis. Note that if a hydrocarbon undergoing oxidation does not contain oxygen (e.g., C_6H_6), coefficient c in Table 2 reactions would be zero, removing it from the reaction.

Table 2. Thermodynamic redox reaction stoichiometry

Aerobic respiration

$$aC(-1) + bH(+1) + cO(-2) + 1.25aO_2 + 0.5(a-c)H_2O \rightarrow aHCO_3^- + (b-2a)H^+$$

Manganese reduction

$$aC(-1) + bH(+1) + cO(-2) + 2.5aMnO_2 + (5a+2c-b)H^+ \rightarrow aHCO_3^- + (2a+c)H_2O$$

Iron reduction

$$aC(-1) + bH(+1) + cO(-2) + 5aFe(OH)_3 + (5a+2c-b)H^+ \rightarrow aHCO_3^- + (12a+c)H_2O$$

Methanogenesis

$$aC(-1) + bH(+1) + cO(-2) + (3d-c)H^+ \rightarrow dHCO_3^- + (b+d-2c-4a)H_2O$$

Surface complexation on $Fe(OH)_3$ was modeled using the generalized two-layer model and database described in Dzombak and Morel[54]. The two-layer model defines "Type 1" and "Type 2" sites, also referred to as strong and weak sites, respectively. $Fe(OH)_3$ strong sites are defined in the PHREEQC database as Hfo_s, where "s" identifies strong sites that correspond to a small subset of surface sites with high affinity for cation sorption. Type 2 sites defined in the PHREEQC database as Hfo_w, where "w" identifies weak sites which correspond to the total reactive sites available for sorption of protons, cations, and anions to $Fe(OH)_3$ as determined by observed sorption maxima[54]. Initial simulations accounted for Co^{2+} sorption reactions to both strong and weak sites, and strong sites were more favored to the point where weak sites did not make a significant impact comparatively. Ni^{2+} sorption reactions were modeled only to strong sites as Dzombak and Morel[54] did not report a logK for a weak site sorption reaction and strong site sorption tends to be more favorable for cations. Arsenic (as oxyanions) and HCO_3^- sorption reactions were modeled using only weak sites, as strong sites are cation-specific. $Fe(OH)_3$ sorption constants where based on values from Dzombak and Morel[54] and then calibrated within the model.

The specific surface area (600 m^2/g) and surface site density for Hfo_s (0.006 mol/mol Fe) (Table 3) were taken from the Dzombak and Morel[54] database.

Sorption onto $FeCO_3$ was modeled using a one-site surface complexation model similar to that explained by Tahervand and Jalali[55]. Binding sites were described by surface complexation reactions combined with surface characteristics such as specific surface area and site density.

Guo[56] found a range of values for the surface area (6.8 – 8.5 m^2/g) of a sample comprised of 96% $FeCO_3$. Because the $FeCO_3$ precipitated in the aquifer is likely highly amorphous, I used the value on the high end of the range from Guo[56] (8.5 m^2/g) [56] and doubled it in the model to a value of 17 $m^2/$ g of $FeCO_3$ (Table 3) to better approximate the high ratio of surface area to volume of amorphous $FeCO_3$. The site density reported by Van Cappellen et al.[57] of 18 μmol sites/m^2 surface area $FeCO_3$[57] combined with the assumption that carbonate surface sites ($>CO_3$) make up half of the sites and result in a surface site density of 9 μmol $>CO_3$ sites/m^2 surface area $FeCO_3$. To achieve similar concentrations and patterns of Ni^{2+} and Co^{2+} sorbed to $FeCO_3$ and to reflect the amorphous nature of $FeCO_3$, the surface site density was doubled to 18 μmol $>CO_3$ sites/m^2 surface area $FeCO_3$ (Table 3).

Current research of carbonate surface complexation has been done in a limited capacity using laboratory experiments and has mainly focused on homogeneous systems (e.g., Mn sorbed to $MnCO_3$, Fe sorbed to $FeCO_3$). The exception to this is calcite ($CaCO_3$), which has been studied in greater detail. Sorption of various cations including Ba^{2+}, Sr^{2+}, Cd^{2+}, Mn^{2+}, Zn^{2+}, Co^{2+}, and Ni^{2+} to calcite is described by Zachara et al.[58]. To my knowledge, logK values for sorption of Co^{2+} and Ni^{2+} to siderite do not exist in the literature. Therefore, I assumed that logK values for sorption to calcite would serve as reasonable initial estimates given the similar mineralogy between calcite and siderite. Thus, logK values for Co^{2+} and Ni^{2+} sorption to calcite from Zachara et al.[58] were put into the model as proxies and then calibrated in the model based on field data from Jones[1] to better reflect sorption parameters onto $FeCO_3$.

Modeled output Ni^{2+} and Co^{2+} concentrations were constrained by new and archival groundwater and sediment chemistry data compiled by Jones[1], while also honoring previously documented patterns of DO, pH, Fe, NVDOC, and BEX constrained by groundwater and sediment chemistry data collected in 1987, 1993, and 2008[28]. DO, pH, and Fe were further constrained by 2011-2015 data[14,15,16].

Table 3. Sorption Parameters and Reactions

Site Density Parameters		Site density			Ref.
	$Fe(OH)_3$	$6\ \frac{\mu mol >OH_3\ sites}{m^2\ surface\ area}$			(a)
	$FeCO_3$	$18\ \frac{\mu mol >CO_3\ sites}{m^2\ surface\ area}$			(b)
Surface Area Parameters		Surface Area			
	$Fe(OH)_3$	$600\ (\frac{m^2}{g\ Fe(OH)_3})$			(a)
	$FeCO_3$	$17\ \frac{m^2}{g\ FeCO_3}$			(c)
		logK	$logK^-$ 95% C.I.^{b}	$logK^+$ 95% C.I.^{c}	ref.
Surface (de)protonation reactions					
Rxn. 1	$Hfo\_wOH + H^+ = Hfo\_wOH_2^+$	7.29			(a)
Rxn. 2	$Hfo\_wOH = Hfo\_wO^- + H^+$	-8.93			(a)
Rxn. 3	$Hfo\_sOH + H^+ = Hfo\_sOH_2^+$	7.29			(a)
Rxn. 4	$Hfo\_sOH = Hfo\_sO- + H^+$	-8.93			(a)
Rxn. 5	$SidH = Sid^- + H^+$	-4.4			(b)
Ni 2+ reactions					
Rxn. 6	$Sid^- + Ni^{2+} = SidNi^+$	-1.3			(g)

Rxn. 7	$Hfo\_sOH + Ni^{2+} = Hfo\_sONi + H^+$	1.5			(b)
Co 2+ surface reactions					
Rxn. 8	$Sid^- + Co^{2+} = SidCo^+$	-1.5			(g)
Rxn. 9	$Hfo\_sOH + Co^{2+} = Hfo\_sOCo + H^+$	1.6			(b)
Rxn. 10	$Hfo\_wOH + Co^{2+} = Hfo\_wOCO^+ + H^+$	-3.01			(a)
Arsenate (As(V)) reaction					
Rxn. 11	$Hfo\_wOH + AsO_4^{3-} + 3H^+ = Hfo\_wH_2AsO_4 + H_2O$	29.31	28.29	30.34	(a)
Rxn. 12	$Hfo\_wOH + AsO_4^{3-} + 2H^+ = Hfo\_wHAsO_4^- + H_2O$	23.51	23.33	23.7	(a)
Rxn. 13	$Hfo\_wOH + AsO_4^{3-} + H^+ = Hfo\_wAsO_4^{2-} + H_2O$	18.1			(e)
Rxn. 14	$Hfo\_wOH + AsO_4^{3-} = Hfo\_wOHAsO_4^{3-}$	10.58	10.01	11.15	(a)
Arsenite (As(III)) reactions					
Rxn. 15	$Hfo\_wOH + H_3AsO_3 = Hfo\_wH_2AsO_3 + H_2O$	5.41	5.11	5.71	(a)
Bicarbonate reaction					
Rxn. 16	$Hfo\_wOH + CO_3^{2-} + 2H^+ = Hfo\_wHCO_3 + H_2O$	20.37	19.39	21.35	(f)
Rxn. 17	$Hfo\_wOH + CO_3^{2-} + H^+ = Hfo\_wCO_3^- + H_2O$	12.78	12.58	12.98	(f)
Acid dissociation reactions*a*					
Rxn. 18	$H_3AsO_4 = H_2AsO_4^- + H^+$	2.24			(d)
Rxn. 19	$H_2AsO_4^- = HAsO_4^{2-} + H^+$	6.96			(d)
Rxn. 20	$HAsO_4^{2-} = AsO_4^{3-} + H^+$	11.5			(d)
Rxn. 21	$H_3AsO_3 = H_2AsO_3^- + H^+$	9.29			

[a]Acidity constants correspond to T = 20-25 °C and I = 0.
[b]Lower 95% confidence interval for logK value
[c]Upper 95% confidence interval for logK value

a. Dzombak and Morel (1990)
b. Calibrated based on Van Capellen (1993)
c. Calibrated based on Guo (2007)
d. Smith and Martell (1976)
e. Dixit and Hering (2003)
f. Appelo et al. (2002)
g. Calibrated based on calcium carbonate sorption LogK's in Zachara et al (1990)

2.3 Initial Conditions

Initial parameters for organic C constituents, initial total C mass, and mass fractions of BEX, toluene, NVDOC, short-chain *n*-alkanes, and long chain *n*-alkanes are from Ng et al[29]. Initial concentrations for dissolved constituents (total carbonates, CH_4, Ca^{2+}, Cl^-, Fe^{2+}, Mg^{2+}, Na^+, DO, Mn^{2+}, N_2, pH) were determined based on data from six sampling periods between 1986 and 1995 of an uncontaminated background well upgradient from the spill site (well 310E in Figure 1), these concentrations are also representative of modern-day background concentrations. Concentrations from these sampling periods were averaged and then equilibrated with calcite and charge-balanced using PHREEQC-2. Concentrations for initial model input of aqueous Ni^{2+} and Co^{2+} remained the same after equilibration at 5.2209×10^{-9} mol/L and 4.968×10^{-10} mol/L, respectively. The left boundary and water table boundary are constant concentration flux boundaries with the initial solution chemistry except Ni^{2+} and Co^{2+} which use recharge concentrations equivalent to background conditions that differ from calibrated initial conditions. Arsenic is not included in recharge solution chemistry at the boundaries because it is below detection (<1 µg/L) in background groundwater.

Initial $Fe(OH)_3$ concentrations were based on the average of background sample measurements using a 0.5 M HCl extraction method[45] and assuming a bulk density of 1650 g/L. The extraction method used targets operationally defined "easily reducible" Fe(III)[45] that is then characterized in the model as $Fe(OH)_3$. The concentration of reducible Fe(III) was determined by comparing the amount of Fe(III) extracted from uncontaminated background sediment to the amount of Fe(III) extracted from sediment just downgradient from the oil body in the contaminant plume. Near the oil body, Fe-reduction has occurred for several years following the spill prior to turning methanogenic after the bioavailable Fe(III) had been depleted. Extraction results showed low amounts of HCl-extractable Fe(III) remain in the sediment near the crude-oil body despite redox conditions being methanogenic, indicating that not all Fe(III) in the sediment may be easily reducible by microbes[16]. Thus, the difference between Fe(III) concentrations in uncontaminated background sediment and sediment near the crude-oil body was used to constrain the initial $Fe(OH)_3$ concentration of 0.0288 mol/L_v (L_v is bulk or total aquifer volume— solids plus pore space— in liters). Similarly, initial concentrations of Ni^{2+} and Co^{2+} sorbed to $Fe(OH)_3$ were constrained by the difference between the background concentrations and residual concentrations near the crude-oil body. Thus, the model represents the concentration of Ni^{2+} and Co^{2+} made available through biodegradation.

The surface complexation model for Ni^{2+} and Co^{2+} was equilibrated with the dissolved concentrations in the initial solution to approximate observed concentrations of Ni^{2+} and Co^{2+} sorbed to $Fe(OH)_3$[1]. The initial concentrations of dissolved Ni^{2+} and Co^{2+} were calibrated to best match concentrations of Ni^{2+} and Co^{2+} in groundwater and sediment while remaining close to background concentrations at 15,000 days to be 5.2209×10^{-9} mol/L and 4.968×10^{-10} mol/L respectively. The groundwater concentration of Ni^{2+} and Co^{2+} for recharge was set to groundwater background levels of 5.6209 x 10^{-9} mol/L and 1.6968 x 10^{-9} mol/L respectively, as reported by Jones[1]. After equilibration, concentrations of Ni^{2+} and Co^{2+} sorbed to $Fe(OH)_3$ where 0.023 mmol/L_v and 0.0027 mmol/L_v respectively. Background conditions for Ni^{2+} and Co^{2+} in sediment from field data are 0.07 mmol/L_v and 0.013 mmol/L_v respectively. Because background groundwater is undersaturated with respect to $FeCO_3$, $FeCO_3$ does not form in background sediment in the model, and thus there are no Ni^{2+} or Co^{2+} complexes on $FeCO_3$ as an initial condition.

2.4 Calibration Approach

The model in this study was calibrated so that patterns of Ni^{2+} and Co^{2+} concentrations in the sediment and groundwater were similar to that of the field data collected from 2010 – 2019[1]; it also honors the spatial concentration patterns of DO, pH, Fe^{2+}, CH_4, $Fe(OH)_3$, and $FeCO_3$ observed in 1987, 1999, 2008, and 2015, which were accounted for in previous versions of this model[19,29]. Given that all these parameters are interdependent upon one another in the equilibrium model, I recognized that concessions regarding spatial patterns of trace elements and simulated concentrations would have to be made to honor the collective processes occurring in the model plume. As such, I decided that simulated concentrations within one order of magnitude of the measured concentrations in the field would constitute an "accurate" model. While I attempt to accurately simulate spatial distribution and concentration of Ni^{2+} and Co^{2+} in both groundwater and sediment, a general replication of the spatial distributions was accepted because concentrations can fluctuate in individual wells with no reflection of geochemical processes in the aquifer due to well construction[59–61] and the purging/sampling procedures[62] used. Thus, comparing point-to-point concentrations for calibration is likely overly prescriptive to gaining insight into the biogeochemical reactions that affect the mobilization and attenuation of Ni^{2+} and Co^{2+} in a contaminated aquifer.

3. Results

3.1 Aquifer Chemistry from Biodegradation

In this paper, I report modeled concentrations 15,000 days after the oil spill for DO, Fe^{2+}, HCO_3^-, CH_4 and pH, as they are relevant to the geochemical processes controlling trace element cycling. Other species were included in the simulation but have little relevance to the cycling of trace elements, so their values are not reported here.

Early aerobic biodegradation of the crude-oil results in depleted DO levels near the oil body (Figure 3.A) and thus allows for the onset of anaerobic biodegradation, namely biodegradation coupled with Fe-reduction and methanogenesis. During Fe-reduction, $Fe(OH)_3$ is reductively dissolved and releases Fe^{2+} into groundwater creating a plume of elevated Fe^{2+} concentrations (Figure 3.E). After the reservoir of $Fe(OH)_3$ has been depleted near the oil body due to Fe-reduction, biodegradation proceeds by methanogenesis, resulting in a plume of elevated dissolved CH_4 concentrations (Figure 3.B). During all biodegradation reactions, organic C is mineralized to produce high concentrations of HCO_3^- (Table 2). Further downgradient from the methanogenic zone, where $Fe(OH)_3$ reduction is the dominant TEAP (~100 m downgradient), elevated dissolved Fe^{2+} combined with elevated HCO_3^- cause groundwater supersaturation with respect to siderite ($FeCO_3$), causing it to precipitate with the highest concentrations from 50 – 100 m downgradient from well 421 (Figure 3.F)(Eq. 1).

$$Fe^{2+} + HCO_3^- = Fe^{2+} + CO_3^{2-} + H^+ = FeCO_3 + H^+ \qquad \text{(Eq. 1)}$$

Multiple reactions, including siderite formation, are pH-dependent, so a discussion of the controls on pH is warranted. Near the oil body, field data have shown abundant non-carbonate Fe(II) in the sediment. This, combined with low pH as seen in field data[1], leads to the use of cation exchange in the model to allow for partially immobilized Fe(II) to appear as FeX_2[29], which produces acidity as a byproduct (Eq. 2).

$$2HX + Fe^{2+} = FeX_2 + 2H^+ \qquad \text{(Eq. 2)}$$

H^+ is a reaction byproduct of methanogenesis (Table 2), a primary TEAP near to the oil body. Combined, methanogenesis and cation exchange explain the lower pH observed -25 - 100 m downgradient from well 421 (Figure 3.D). Further downgradient in the Fe-reducing zone, H^+ is consumed as a reactant during Fe-reduction (Table 2), leading to an overall increase in pH as a result of the reaction. Lower pH (i.e., elevated concentrations of H^+) thermodynamically disfavors the formation of $FeCO_3$ near the oil, as H^+ is a product of siderite precipitation from Fe^{2+} and HCO_3^- (Eq.1). Despite the higher concentrations of Fe^{2+} (Figure 3.E) and HCO_3^- (Figure 3.G) closer to the oil, the higher concentrations of H^+ in this zone thermodynamically limit siderite from forming. This results in the highest siderite concentrations in the Fe-reducing zone (Figure 3.F), even though Fe^{2+} and HCO_3^- concentrations are comparatively lower in groundwater in this zone.

Last, the resulting pH controls the surface charge on the two sorbent phases, $Fe(OH)_3$ and $FeCO_3$, and thus controls their ability to sorb oppositely charged ions in solution. From Table 3, the pK_{a1} and pK_{a2} for $Fe(OH)_3$ are 7.29 and 8.93[54], respectively, meaning that below pH 7.29, the dominant surface charge will be positive, between pH 7.29 and 8.29 the dominant surface charge will be neutral, and above pH 8.29, the dominant surface charge will be negative. However, it is important to note that between pH 7.29 and 8.29, small fractions of both positive and negative surface species exist[63], allowing for surface complexation of both cations and anions simultaneously. From Table 3, the pK_a for $FeCO_3$ is 4.4 meaning that below pH 4.4 the dominant surface charge will be neutral and above pH 4.4 the dominant surface charge will be negative[57]. Near the oil body where methanogenic conditions dominate, pH is lower (~6.6) than background conditions (Figure 3.D). Under these conditions, $Fe(OH)_3$ would generate mostly positively charged surface sites, favoring anion sorption and disfavor sorption of trace element cations. Conversely, $FeCO_3$ would generate a negative surface charge, allowing it to sorb cations. Further downgradient in the Fe-reducing zone, pH is ~6.9-7.3, indicating that the majority of $Fe(OH)_3$ surface sites would be positively charged and favor anion sorption, though some surface sites can be negatively charged and sorb cations. $FeCO_3$ surface sites would be negatively charged and favor cation sorption.

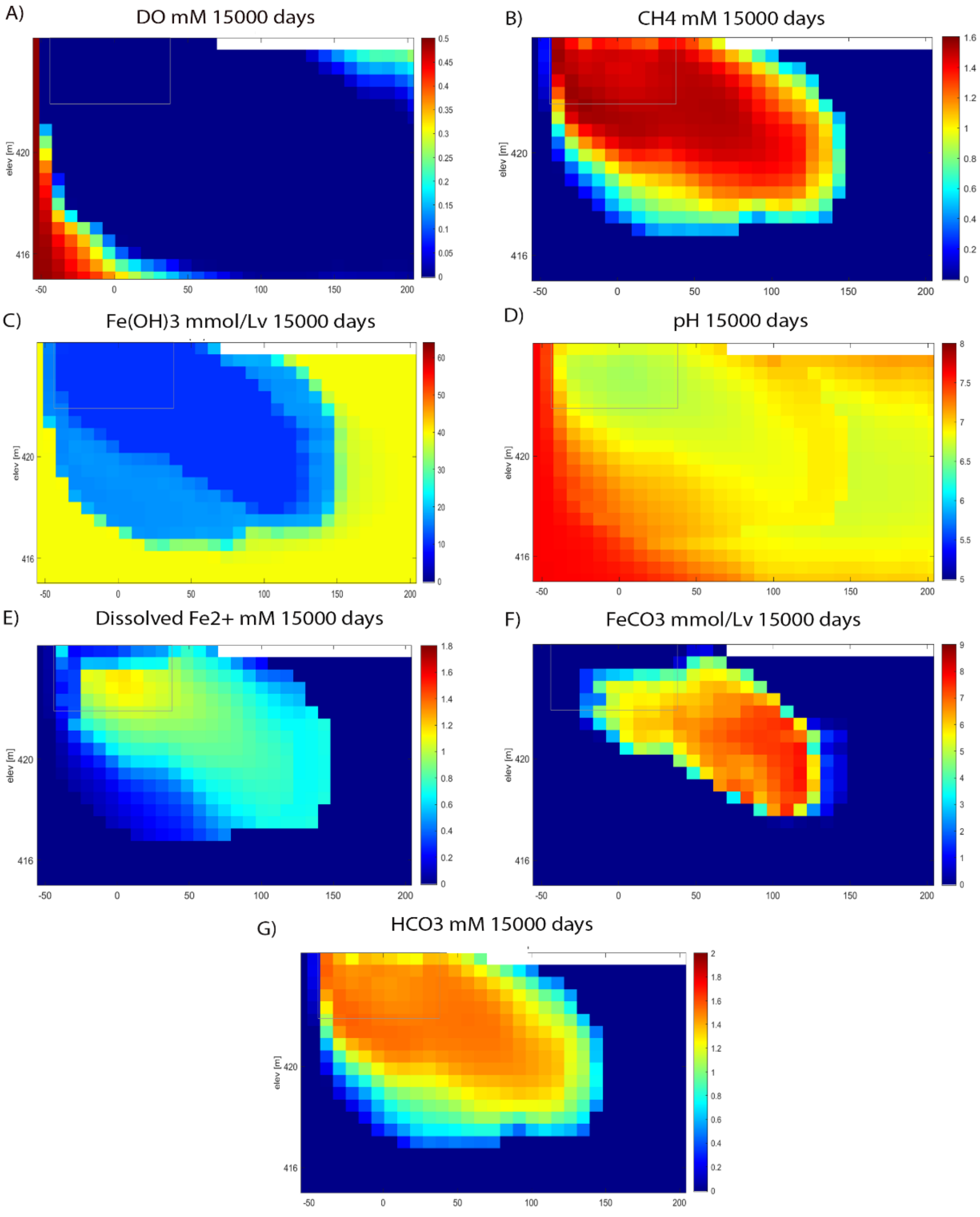

Figure 3. Aquifer chemistry related to biodegradation processes 15,000 days after the oil spill. Constituents include A) dissolved oxygen (mM), B) CH_4 (mM), C) $Fe(OH)_3$ in sediment (mmol/L_v), D) pH, E) aqueous Fe^{2+} (mM), F) $FeCO_3$ in sediment (mmol/L_v).

3.2 Mobilization and Attenuation of Ni^{2+} and Co^{2+}

Here I present results of aqueous and sorbed (to $Fe(OH)_3$ and $FeCO_3$) Ni^{2+} and Co^{2+} phases from the model and compare them to concentrations measured in groundwater and aquifer sediments reported by Jones[1]. Interpolated field data of sediment from Jones[1] represents bulk sediment data (Figure 4.A; 5.A), that includes both available (i.e., mobilizable due to biodegradation processes) and non-available (i.e., Ni and Co remaining in sediment for ~40 years after the spill) Ni and Co in the sediment. Since this residual Ni and Co remain in sediment ~40 years after the spill, I assumed they are likely part of a more recalcitrant mineral phase that is not influenced by biodegradation processes in the plume. Therefore, to make more accurate comparisons of available Ni and Co and model results, the residual concentrations of Ni and Co in sediment near the oil body were subtracted from bulk Ni and Co sediment concentrations in the model domain, resulting in the amount of "available" Ni and Co in sediment that can be mobilized during biodegradation processes (Figure 4B; 5B). These resulting residual-subtraction concentrations of Ni and Co where then used for comparison to the model. It is important to note that the residual-subtraction plots do not specify any specific retention mechanism or phase. In order to illustrate the roles of sorption on $FeCO_3$ and $Fe(OH)_3$ individually, the model produces a plot indicating Ni and Co sorbed to $FeCO_3$ and a separate plot indicating Ni and Co sorbed to $Fe(OH)_3$. The true "total" Ni and Co in sediment in a model cell would be the sum of the metals sorbed to $FeCO_3$ and the metals sorbed to $Fe(OH)_3$, though no cell appears to have appreciable amounts of metals simultaneously sorbed to both minerals, as the two minerals are stable under opposing redox conditions.

Near the crude-oil body, Ni^{2+} and Co^{2+} are depleted in the sediment for two reasons. First, methanogenesis is the primary TEAP because a majority of the available Fe(III) had been reduced in the past, when Fe-reduction was the dominant TEAP in this zone[30]. Ni^{2+} and Co^{2+}, which were originally sorbed to $Fe(OH)_3$ in sediments, were mobilized into groundwater as the hydroxides dissolved. This is reflected by increased concentrations of aqueous Ni^{2+} and Co^{2+} near the oil body (Figure 6). Second, as methanogenic conditions became predominant, and Fe^{2+} exchanged with H^+ in sediment, groundwater pH decreased to values that generate only positive surface charge on $Fe(OH)_3$ based on the pK_{a1} value of 7.29. Although there is some residual $Fe(OH)_3$ near the oil body (Figure 3.C), the surface sites would electrostatically repulse positively charged Ni^{2+} and Co^{2+}, causing them to desorb into groundwater and create their respective plumes.

In the model, the center of mass in the Ni^{2+} groundwater plume is near 50 m downgradient from well 421 and at an elevation of 421 m AMSL with a maximum concentration of 0.0025 mmol/L (Figure 6.B). Field data show the center of mass in the Ni^{2+} groundwater plume is closer to 25 m downgradient from well 421 and at an elevation of 422 m AMSL with a maximum concentration of 0.002 mmol/L[1] (Figure 3.A). The center of mass in the Co^{2+} groundwater plume is near 60 m downgradient from well 421 and at an elevation of 421.5 m with a maximum concentration of 0.00041 mmol/L (Figure 3.D). Field data show the center of mass in the Co^{2+} groundwater plume is near 0 m downgradient from well 421 and at an elevation of 422.5 m AMSL with a maximum concentration of 0.0004 mmol/L[1] (Figure 3.C).

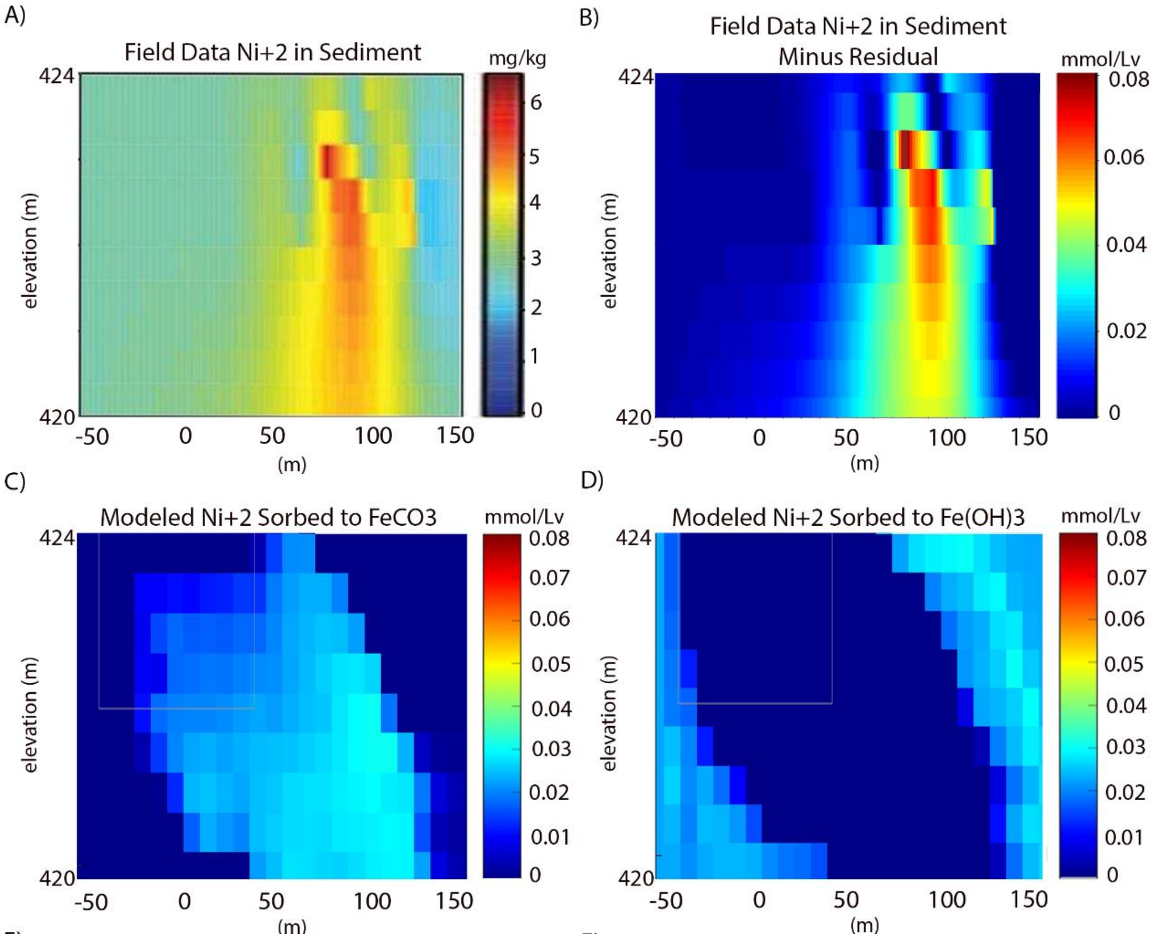

Figure 4 Measured and modeled Ni^{2+} in sediment. A) is a plot of interpolated field data of Ni^{2+} in sediment (mg/kg)from Jones. B) is a plot of interpolated field data of Ni^{2+} in sediment with the residual value of 2.75 mg/kg subtracted and data converted to the model units of mmol/L_v. C) is a plot of modeled Ni^{2+} sorbed to $FeCO_3$ in sediment (mmol/L_v). D) is a plot of modeled Ni^{2+} sorbed to $Fe(OH)_3$ in sediment (mmol/L_v).

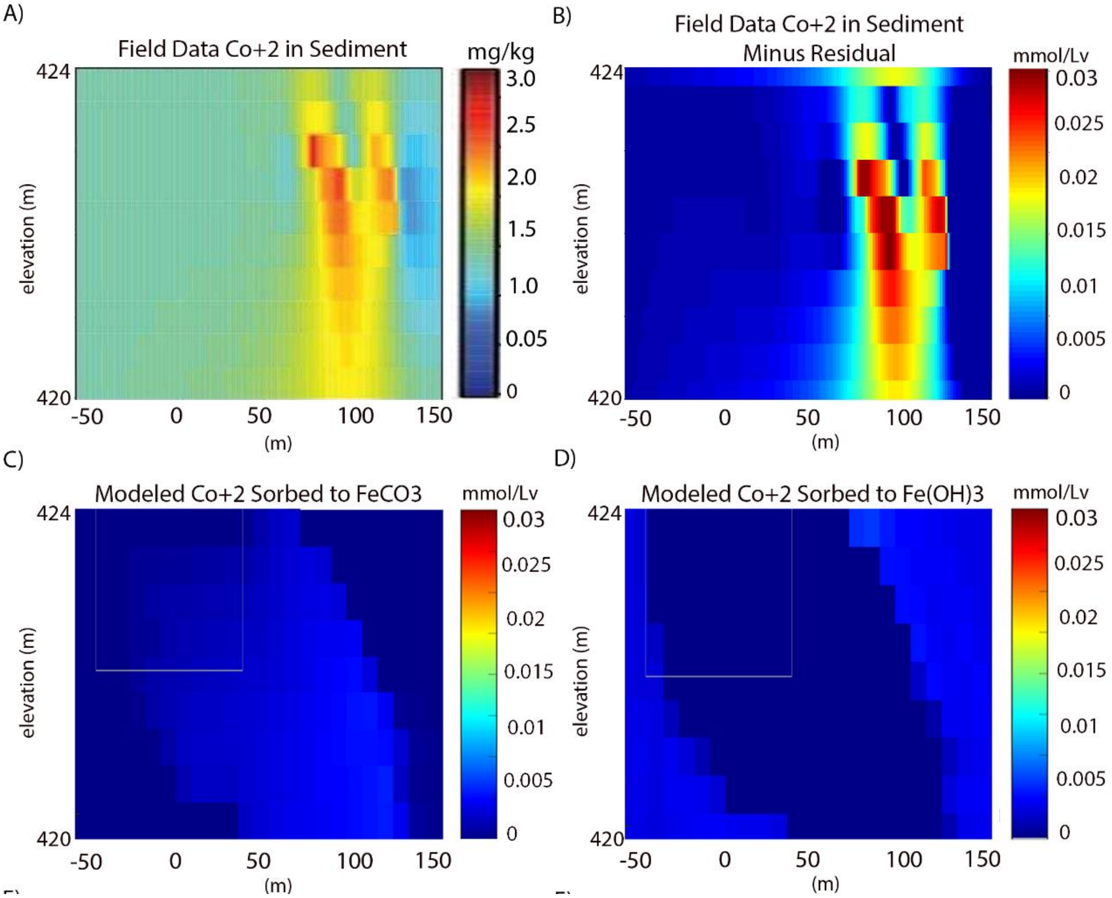

Figure 5 Measured and modeled Co^{2+} in sediment. A) is a plot of interpolated field data of Co^{2+} in sediment from Jones (2020). B) is a plot of interpolated field data of Co^{2+} in sediment with the residual value of 1.25 mg/kg subtracted. C) is a plot of modeled Co^{2+} sorbed to $FeCO_3$ in sediment keeping a consistent color bar range with field data. D) is a plot of modeled Co^{2+} sorbed to $Fe(OH)_3$ in sediment keeping a consistent color bar range with field data. E) is a plot of modeled Co^{2+} sorbed to $FeCO_3$ in sediment with a unique color bar range to highlight the concentrations found in the aquifer. F) is a plot of modeled Co^{2+} sorbed to $FeCO_3$ in sediment with a unique color bar range to highlight the concentrations found in the aquifer

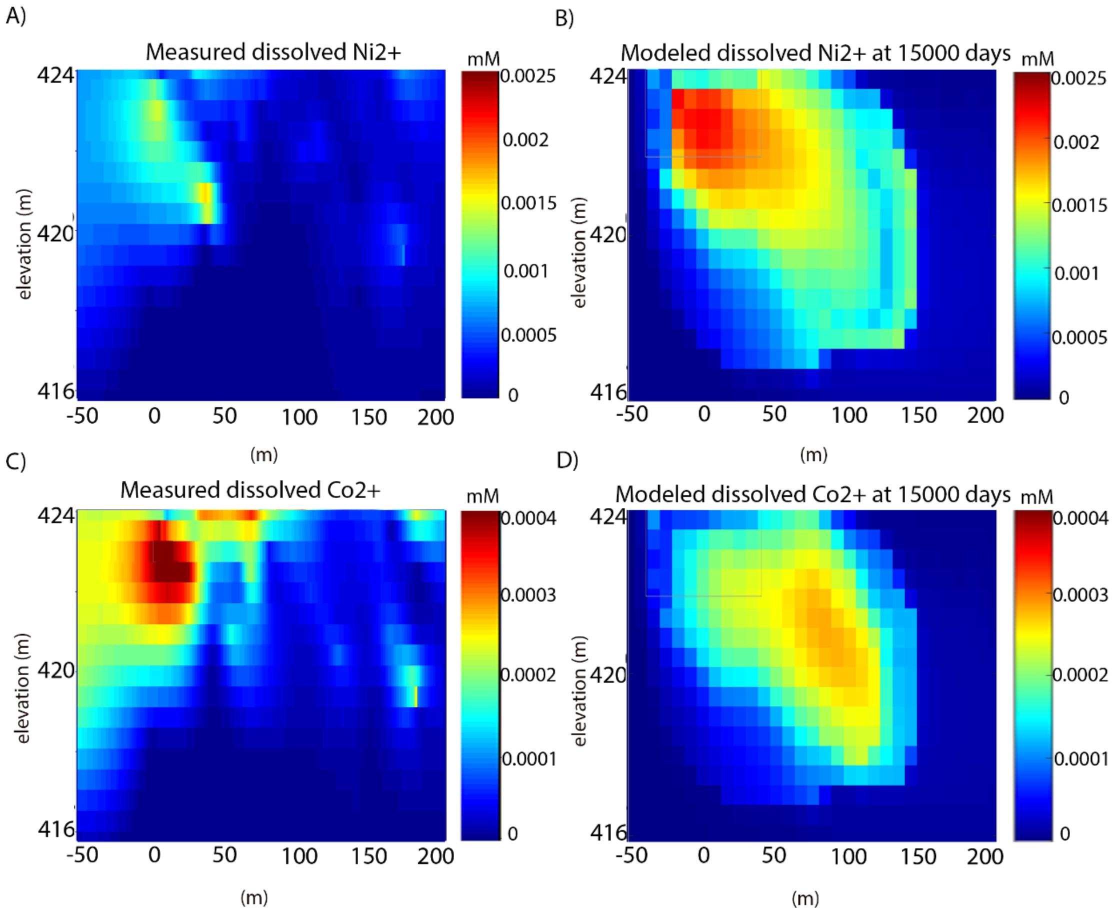

Figure 6. Mobilized trace elements measured from well sampling and modeled in this study. A) is a plot of interpolated measurements of aqueous Ni^{2+} (mM) in the aquifer from Jones[1]. B) is a plot of modeled aqueous Ni^{2+} (mM) in the aquifer. C) is a plot of interpolated measurements of aqueous Co^{2+} (mM) in the aquifer from Jones[1]. D) is a plot of modeled aqueous Co^{2+} (mM) in the aquifer.

From field sampling, Jones[1] observed enrichment of of Ni^{2+} and Co^{2+} in sediment of the Fe-reducing zone and hypothesized that carbonates may be precipitating and sorbing cations. I was able to replicate this hypothesis in the model (Figure 3.F), lending support to Jones' hypothesis.

Increased concentrations of aqueous Fe^{2+} and HCO_3^-, a result of geochemical mechanisms described previously (Table 2), result in the precipitation of $FeCO_3$, and at the pH values present in the Fe-reducing zone (Figure 3.D), $FeCO_3$ generates a negative surface charge (Table 2) allowing Ni^{2+} and Co^{2+} to sorb onto siderite in the sediment. Thus at 15,000 days, Ni^{2+} and Co^{2+} are largely attenuated by sorption from 0 - 100 m downgradient from well 421 with the highest concentrations occurring in the Fe-reducing zone between 50 – 100 m downgradient from well 421 via this mechanism. The maximum concentrations of Ni^{2+} and Co^{2+} sorbed to $FeCO_3$ at 15,000 days are 0.03 mmol/L_v and 0.0041 mmol/L_v, respectively (Figures 4 and 5), and are slightly lower than concentrations seen in field data of 0.08 mmol/L_v and 0.03 mmol/L_v, respectively[1].

The model indicates a greater attenuation of Ni^{2+} and Co^{2+} via sorption to $FeCO_3$ near the oil body than is observed in field data, perhaps because groundwater pH in the model is ~0.5-0.75 pH units higher than observed in groundwater near the oil, diminishing the effect of low pH inhibition of siderite precipitation (Eq. 1) while simultaneously increasing the relative abundance of negative surface sites able to sorb Ni^{2+} and Co^{2+}. Regardless, the model demonstrates an overall depletion of Ni and Co concentrations in sediment in this region relative to background concentrations, consistent with the pattern observed from field sampling; both modeled data and field data reflect regions of high concentrations of Ni^{2+} and Co^{2+} in sediment in the Fe-reducing zone and at the leading edge of the plume, caused by the precipitation of $FeCO_3$ and $Fe(OH)_3$, respectively. Both of these minerals serve as sorbent phases for Ni^{2+} and Co^{2+} based on the pH in their respective zones.

Further downgradient where the aquifer transitions from anoxic Fe-reducing zone to suboxic conditions, groundwater is no longer supersaturated with respect to $FeCO_3$, so its precipitation ceases (Figure 3.D). Additionally, the suboxic conditions result in the oxidizing of aqueous Fe^{2+}

and precipitate $Fe(OH)_3$, which in turn attenuates Ni^{2+} and Co^{2+} through sorption. At ~125 m downgradient from well 421, a "wall" of elevated concentrations of Ni^{2+} and Co^{2+} sorbed to $Fe(OH)_3$ in sediment occurs (Figures 4 and 5), because $Fe(OH)_3$ is stable under the suboxic conditions and the pH allows for the formation of negatively charged surface sites. The maximum concentrations of Ni^{2+} and Co^{2+} sorbed to the wall of precipitated $Fe(OH)_3$ at 15,000 days are 0.02 mmol/L_v and 0.003 mmol/L_v respectively. The maximum concentrations of Ni^{2+} and Co^{2+} in sediment from field data are 0.08 mmol/L_v and 0.03 mmol/L_v, respectively[1].

4.1 Discussion

Concentrations and patterns in the model reflect the same general patterns observed in field data, but the model could not exactly match the field data due to the comprehensive modeling approach of simulating numerous parameters for 40+ years of data with reasonable accuracy. The sediment concentrations can be more closely matched to field data using different logK values, but this match occurs at the expense of not only groundwater concentrations but the location of the groundwater plume as well. Thus, a model that is not an exact match but is close to both sediment concentrations as well as groundwater plume location was considered accurate.

While extensive research of sorption parameters for $Fe(OH)_3$ exist[54], this model illustrates the need for a better understanding of sorption parameters related to $FeCO_3$, especially in contaminant plumes where Fe-reduction occurs. Some research has looked at the surface area and site density of $FeCO_3$[56,57] though these laboratory findings likely do not reflect the surface area of amorphous $FeCO_3$ precipitates that form in a complex geochemical environment like the Bemidji contaminant plume. Little research has been done to determine sorption constants for Ni^{2+} or Co^{2+} sorption to siderite. A more robust understanding of sorption parameters for $FeCO_3$ much like that of $Fe(OH)_3$ is essential to better understand mobilization and attenuation of trace elements in crude-oil contaminated aquifers and more generally in aquifers with abundant bioavailable organic carbon that biodegrades via Fe-reduction.

Parameterizing $FeCO_3$ is further complicated by the fact that the actual Fe carbonate phase has been difficult to characterize in the Bemidji aquifer. It has been particularly difficult to positively identify crystalline Fe-carbonates in sediment from the field (Ziegler, personal communication), likely due to its amorphous or poorly crystalline nature. This is congruent with expectations for recently precipitated $FeCO_3$. Kohler et al.[64] looked at two sediment cores from the Fe-reducing zone of Bemidji contaminant plume. Each of these cores contained Fe^{2+} attributed to ion exchangeable and/or carbonate reservoirs. By performing an extraction step that inhibits carbonate dissolution it was possible to determine the amount of Fe^{2+} from a reservoir other than ion exchange, possibly a carbonate reservoir such as siderite, ferroan calcite, or an amorphous phase. Because the carbonate phase(s) is not well characterized, it is difficult to determine model inputs for its mineral properties (i.e. surface area, surface side density, and reactivity).

There are multiple surface complexation models that can be used in a reactive transport model. Previous modeling studies have used the constant-capacitance model[65], the diffuse-layer model[54], the triple-layer model[66], and the charge distribution multisite surface complexation (CD-MUSIC) model[67]. The constant-capacitance model assumes a sorption mechanism of ligand exchange for anionic trace elements that sorb and form tightly bound inner-sphere complexes[68]. The diffuse-layer model, also known as the double-layer model, assumes inner-sphere surface complexes are formed but also includes a diffuse layer formed by background electrolyte ions[68]. Surface complexation of $Fe(OH)_3$ has been successfully modeled at the Bemidji aquifer[69] with surface parameters from Dzombak and Morel[54] using the double-layer model thus the same was used in this model. The triple-layer model assumes inner-sphere complexation occurs as well as adsorption through an outer-sphere adsorption mechanism that results in weaker surface complexes[68]. The CD-MUSIC model assumes inner- and outer-sphere complexes are possible but also allows for various reactive surface groups including singly, doubly, and triply coordinated hydroxyl groups[68]. These more specific surface complexation models were considered for $FeCO_3$ in this model. However, due to the lack of studies on surface parameters for $FeCO_3$, these more specific models were determined to be over-parameterized for modeling trace element sorption to $FeCO_3$ in this study.

Geogenic trace elements like Ni^{2+} and Co^{2+} commonly occur in aquifer solids, through sorption to Fe hydroxides. However, when bioavailable organic C is introduced into the system, biodegradation processes can result in the mobilization trace elements through Fe-reduction and create secondary trace element contaminant plumes. In the Bemidji aquifer, we observed this phenomenon with respect to Ni^{2+} and Co^{2+} while others have also observed the mobilization of As and Ba^{2+} and Sr^{2+}. However, it is important to recognize that trace element mobilization is not limited to just these particular trace elements. In fact, the potential for trace element mobilization is dependent upon the trace elements originally sorbed to the Fe hydroxide in the aquifer matrix. For example, lead, cadmium, and mercury were non-detectable in uncontaminated sediments in the Bemidji aquifer, therefore they likely would not pose a groundwater threat. However, it is possible that an aquifer with higher levels of naturally occurring lead, cadmium, or mercury in sediment is vulnerable to unsafe groundwater concentrations of these toxic elements if reducing conditions are established.

Complex mixtures of trace elements in groundwater can have unique ecological health consequences and human health impacts via drinking water. In the contaminated portion of the Bemidji aquifer, aqueous Ni^{2+} exceeds regulatory limits. Excess Ni^{2+} has been linked to skin irritation[21]. Though Co^{2+} is not currently regulated by the EPA, it is under consideration due to its possible public health concerns[23]. Furthermore, more research is needed to understand the combined toxicology of simultaneous exposure to benzene, Ni^{2+}, Co^{2+}, and other mobilized trace elements[70] .This model underscores the importance of monitoring not only organic contaminants at crude-oil spill sites but inorganic contaminant, and particularly trace elements, as well.

5. Conclusion

This model describes the geochemical processes behind mobilization and attenuation of geogenic trace elements triggered by biodegradation processes. Reducing conditions in the aquifer lead to biodegradation coupled with Fe-reduction which causes the dissolution of $Fe(OH)_3$ and mobilizes trace elements such as Ni^{2+} and Co^{2+} that were previously sorbed to $Fe(OH)_3$ in the aquifer matrix. Within the active Fe-reducing zone groundwater becomes saturated with respect to $FeCO_3$ leading to its precipitation. Given the conditions of the aquifer where $FeCO_3$ precipitates, it generates a negative surface charge and thus is capable of attenuating previously mobilized cations while allowing mobilized oxyanions (such as As) to remain in groundwater. Downgradient, conditions are no longer favorable for siderite but are favorable for the precipitation of $Fe(OH)_3$, allowing for the sorption of both cations and oxyanions including Ni^{2+}, Co^{2+}, and As based on its simultaneous positively and negatively charged surface sites. Conditions in the active Fe-reducing zone which allow for the precipitation and negative surface charge of $FeCO_3$ can, in part, account for the similarities in Ni^{2+} and Co^{2+} attenuation patterns in the aquifer as well as the differences in Ni^{2+}/Co^{2+} and As attenuation patterns in the aquifer. This modeling study highlights the importance in expanding our knowledge of $FeCO_3$ sorption parameters as well as the importance of monitoring inorganic contaminants, specifically trace elements, at organic contaminant sites.

Acknowledgements

I would like to thank Gene-Hua Crystal Ng, who provided valuable insights into the robust Bemidji site model that was adapted in this study. I would also like to thank Isabelle Cozzarelli, who offered insight into trace-element cycling in the aquifer. I am grateful to Kurt Knesel for his insightful comments and suggestions on earlier drafts of this thesis. Finally, I would like to express special thanks to Brady Ziegler for advising me on this thesis project.

References

(1) Jones, K. L. Trace Element Cycling in Crude-Oil-Contaminated Aquifer near Bemidji, Northern Minnesota., Trinity University, San Antonio, TX, 2020.

(2) Toccalino, P. L.; Hopple, J. A. *The Quality of Our Nation's Waters—Quality of Water from Public-Supply Wells in the United States, 1993–2007—Overview of Major Findings: U.S. Geological Survey Circular 1346*; 2010.

(3) Zachara, J. M.; Fredrickson, J. K.; Smith, S. C.; Gassman, P. L. Solubilization of Fe (III) Oxide-Bound Trace Metals by a Dissimilatory Fe (III) Reducing Bacterium. *Geochimica et Cosmochimica Acta* **2001**, *65* (1), 75–93.

(4) Buschmann, J.; Berg, M.; Stengel, C.; Winkel, L.; Sampson, M. L.; Trang, P. T. K.; Viet, P. H. Contamination of Drinking Water Resources in the Mekong Delta Floodplains: Arsenic and Other Trace Metals Pose Serious Health Risks to Population. *Environment International* **2008**, *34* (6), 756–764.

(5) Nickson, R.; McArthur, J.; Burgess, W.; Ahmed, K. M.; Ravenscroft, P.; Rahmanñ, M. Arsenic Poisoning of Bangladesh Groundwater. *Nature* **1998**, *395* (6700), 338.

(6) Kjøller, C.; Postma, D.; Larsen, F. Groundwater Acidification and the Mobilization of Trace Metals in a Sandy Aquifer. *Environmental science & technology* **2004**, *38* (10), 2829–2835.

(7) Yang, J. Y.; Yang, X. E.; He, Z. L.; Li, T. Q.; Shentu, J. L.; Stoffella, P. J. Effects of PH, Organic Acids, and Inorganic Ions on Lead Desorption from Soils. *Environmental Pollution* **2006**, *143* (1), 9–15.

(8) Houben, G. J.; Sitnikova, M. A.; Post, V. E. A. Terrestrial Sedimentary Pyrites as a Potential Source of Trace Metal Release to Groundwater–A Case Study from the Emsland, Germany. *Applied Geochemistry* **2017**, *76*, 99–111.

(9) Zhang, Y.-C.; Slomp, C. P.; Broers, H. P.; Passier, H. F.; van Cappellen, P. Denitrification Coupled to Pyrite Oxidation and Changes in Groundwater Quality in a Shallow Sandy Aquifer. *Geochimica et Cosmochimica Acta* **2009**, *73* (22), 6716–6726.

(10) Schreiber, M. E.; Simo, J. A.; Freiberg, P. G. Stratigraphic and Geochemical Controls on Naturally Occurring Arsenic in Groundwater, Eastern Wisconsin, USA. *Hydrogeology Journal* **2000**, *8* (2), 161–176.

(11) Aksoy, N.; Şimşek, C.; Gunduz, O. Groundwater Contamination Mechanism in a Geothermal Field: A Case Study of Balcova, Turkey. *Journal of Contaminant Hydrology* **2009**, *103* (1–2), 13–28.

(12) Morales, I.; Villanueva-Estrada, R. E.; Rodríguez, R.; Armienta, M. A. Geological, Hydrogeological, and Geothermal Factors Associated to the Origin of Arsenic, Fluoride, and Groundwater Temperature in a Volcanic Environment "El Bajío Guanajuatense", Mexico. *Environmental Earth Sciences* **2015**, *74* (6), 5403–5415.

(13) Brammer, H.; Ravenscroft, P. Arsenic in Groundwater: A Threat to Sustainable Agriculture in South and South-East Asia. *Environment International* **2009**, *35* (3), 647–654. https://doi.org/https://doi.org/10.1016/j.envint.2008.10.004.

(14) Cozzarelli, I. M.; Schreiber, M. E.; Erickson, M. L.; Ziegler, B. A. Arsenic Cycling in Hydrocarbon Plumes: Secondary Effects of Natural Attenuation. *Groundwater* **2016**, *54* (1), 35–45. https://doi.org/10.1111/gwat.12316.

(15) Ziegler, B. A.; Schreiber, M. E.; Cozzarelli, I. M.; Crystal Ng, G.-H. A Mass Balance Approach to Investigate Arsenic Cycling in a Petroleum Plume. *Environmental Pollution* **2017**, *231*, 1351–1361. https://doi.org/https://doi.org/10.1016/j.envpol.2017.08.110.

(16) Ziegler, B. A.; Schreiber, M. E.; Cozzarelli, I. M. The Role of Alluvial Aquifer Sediments in Attenuating a Dissolved Arsenic Plume. *Journal of Contaminant Hydrology* **2017**, *204*, 90–101. https://doi.org/https://doi.org/10.1016/j.jconhyd.2017.04.009.

(17) Amirbahman, A.; Kent, D. B.; Curtis, G. P.; Davis, J. A. Kinetics of Sorption and Abiotic Oxidation of Arsenic(III) by Aquifer Materials. *Geochimica et Cosmochimica Acta* **2006**, *70* (3), 533–547. https://doi.org/https://doi.org/10.1016/j.gca.2005.10.036.

(18) Delemos, J. L.; Bostick, B. C.; Renshaw, C. E.; StÜrup, S.; Feng, X. Landfill-Stimulated Iron Reduction and Arsenic Release at the Coakley Superfund Site (NH). *Environmental science & technology* **2006**, *40* (1), 67–73.

(19) Ziegler, B. A.; McGuire, J. T.; Cozzarelli, I. M. Rates of As and Trace-Element Mobilization Caused by Fe Reduction in Mixed BTEX–Ethanol Experimental Plumes. *Environmental Science & Technology* **2015**, *49* (22), 13179–13189. https://doi.org/10.1021/acs.est.5b02341.

(20) Kravchenko, J.; Darrah, T. H.; Miller, R. K.; Lyerly, H. K.; Vengosh, A. A Review of the Health Impacts of Barium from Natural and Anthropogenic Exposure. *Environmental*

Geochemistry and Health **2014**, *36* (4), 797–814. https://doi.org/10.1007/s10653-014-9622-7.

(21) Nielsen, G. D.; Søderberg, U.; Jørgensen, P. J.; Templeton, D. M.; Rasmussen, S. N.; Andersen, K. E.; Grandjean, P. Absorption and Retention of Nickel from Drinking Water in Relation to Food Intake and Nickel Sensitivity. *Toxicology and Applied Pharmacology* **1999**, *154* (1), 67–75. https://doi.org/https://doi.org/10.1006/taap.1998.8577.

(22) Smith, A. H.; Hopenhayn-Rich, C.; Bates, M. N.; Goeden, H. M.; Hertz-Picciotto, I.; Duggan, H. M.; Wood, R.; Kosnett, M. J.; Smith, M. T. Cancer Risks from Arsenic in Drinking Water. *Environmental Health Perspectives* **1992**, *97*, 259–267. https://doi.org/10.1289/ehp.9297259.

(23) US EPA, O. Announcement of Preliminary Regulatory Determinations for Contaminants on the Fourth Drinking Water Contaminant Candidate List. **2020**.

(24) Baedecker, M. J.; Cozzarelli, I. M.; Eganhouse, R. P.; Siegel, D. I.; Bennett, P. C. Crude Oil in a Shallow Sand and Gravel Aquifer—III. Biogeochemical Reactions and Mass Balance Modeling in Anoxic Groundwater. *Applied Geochemistry* **1993**, *8* (6), 569–586. https://doi.org/https://doi.org/10.1016/0883-2927(93)90014-8.

(25) Bennett, P. C.; Siegel, D. E.; Baedecker, M. J.; M.F., H. Crude Oil in a Shallow Sand and Gravel Aquifer—I. Hydrogeology and Inorganic Geochemistry. *Applied Geochemistry* **1993**, *8* (6), 529–549. https://doi.org/https://doi.org/10.1016/0883-2927(93)90012-6.

(26) Hult, M. F.; (U.S.), G. S. *Ground-Water Contamination by Crude Oil at the Bemidji, Minnesota, Research Site: U.S. Geological Survey Toxic Waste--Ground-Water Contamination Study : Papers Presented at the Toxic-Waste Technical Meeting, Tucson, Arizona, March 20-22, 1984*; Ground-water Contamination by Crude Oil at the Bemidji, Minnesota, Research Site: U.S. Geological Survey Toxic Waste--ground-water Contamination Study : Papers Presented at the Toxic-Waste Technical Meeting, Tucson, Arizona, March 20-22, 1984; U.S. Geological Survey, 1984.

(27) Essaid, H.; Bekins, B.; Herkelrath, W.; Delin, G. Crude Oil at the Bemidji Site: 25 Years of Monitoring, Modeling, and Understanding. *Ground water* **2009**, *49*, 706–726. https://doi.org/10.1111/j.1745-6584.2009.00654.x.

(28) Ng, G.-H. C.; Bekins, B. A.; Cozzarelli, I. M.; Baedecker, M. J.; Bennett, P. C.; Amos, R. T. A Mass Balance Approach to Investigating Geochemical Controls on Secondary Water Quality Impacts at a Crude Oil Spill Site near Bemidji, MN. *Journal of Contaminant Hydrology* **2014**, *164*, 1–15. https://doi.org/https://doi.org/10.1016/j.jconhyd.2014.04.006.

(29) Ng, G.-H. C.; Bekins, B. A.; Cozzarelli, I. M.; Baedecker, M. J.; Bennett, P. C.; Amos, R. T.; Herkelrath, W. N. Reactive Transport Modeling of Geochemical Controls on Secondary Water Quality Impacts at a Crude Oil Spill Site near Bemidji, MN. *Water Resources Research* **2015**, *51* (6), 4156–4183. https://doi.org/https://doi.org/10.1002/2015WR016964.

(30) Cozzarelli, I. M.; Schreiber, M. E.; Erickson, M. L.; Ziegler, B. A. Arsenic Cycling in Hydrocarbon Plumes: Secondary Effects of Natural Attenuation. *Groundwater* **2016**, *54* (1), 35–45. https://doi.org/10.1111/gwat.12316.

(31) Essaid, H. I.; Bekins, B. A.; Godsy, E. M.; Warren, E.; Baedecker, M. J.; Cozzarelli, I. M. Simulation of Aerobic and Anaerobic Biodegradation Processes at a Crude Oil Spill Site. *Water Resources Research* **1995**, *31* (12), 3309–3327.

(32) Essaid, H. I.; Cozzarelli, I. M.; Eganhouse, R. P.; Herkelrath, W. N.; Bekins, B. A.; Delin, G. N. Inverse Modeling of BTEX Dissolution and Biodegradation at the Bemidji, MN Crude-Oil Spill Site. *Journal of Contaminant Hydrology* **2003**, *67* (1), 269–299. https://doi.org/https://doi.org/10.1016/S0169-7722(03)00034-2.

(33) Amos, R. T.; Ulrich Mayer, K. Investigating the Role of Gas Bubble Formation and Entrapment in Contaminated Aquifers: Reactive Transport Modelling. *Journal of Contaminant Hydrology* **2006**, *87* (1), 123–154. https://doi.org/https://doi.org/10.1016/j.jconhyd.2006.04.008.

(34) Curtis, G. P.; Cozzarelli, I. M.; Baedecker, M. J.; Bekins, B. A. Coupled Biogeochemical Modeling of Ground Water Contamination at the Bemidji Minnesota Crude Oil Spill Site. *US Geological Survey Toxic Substances Hydrology Program Proceedings* **1999**, 153–158.

(35) Curtis, G. P. Comparison of Approaches for Simulating Reactive Solute Transport Involving Organic Degradation Reactions by Multiple Terminal Electron Acceptors. *Computers & Geosciences* **2003**, *29* (3), 319–329.

(36) Prommer, H.; Barry, D. A.; Zheng, C. MODFLOW/MT3DMS-Based Reactive Multicomponent Transport Modeling. *Groundwater* **2003**, *41* (2), 247–257. https://doi.org/https://doi.org/10.1111/j.1745-6584.2003.tb02588.x.

(37) Parkhurst, D. L.; Appelo, C. A. J. *USER'S GUIDE TO PHREEQC (VERSION 2)-A COMPUTER PROGRAM FOR SPECIATION, BATCH-REACTION, ONE-DIMENSIONAL TRANSPORT, AND INVERSE GEOCHEMICAL CALCULATIONS*; Denver, Co, 1999.

(38) Harbaugh, A. W. *MODFLOW-2005, The U.S. Geological Survey Modular Ground-Water Model-the Ground-Water Flow Process*; 2005. https://doi.org/https://doi.org/10.3133/tm6A16.

(39) Zheng, C.; Wang, P. P. *MT3DMS: A Modular Three-Dimensional Multispecies Transport Model for Simulation of Advection, Dispersion, and Chemical Reactions of Contaminants in Groundwater Systems; Documentation and User's Guide*; 1999.

(40) Dillard, L. A.; Essaid, H. I.; Herkelrath, W. N. Multiphase Flow Modeling of a Crude-Oil Spill Site with a Bimodal Permeability Distribution. *Water Resources Research* **1997**, *33* (7), 1617–1632. https://doi.org/10.1029/97WR00857.

(41) Strobel, M. L.; Delin, G. N.; Munson, C. J. *Spatial Variation in Saturated Hydraulic Conductivity of Sediments at a Crude-Oil Spill Site near Bemidji, Minnesota*; US Department of the Interior, US Geological Survey, 1998; Vol. 98.

(42) Eganhouse, R. P.; Baedecker, M. J.; Cozzarelli, I. M.; Aiken, G. R.; Thorn, K. A.; Dorsey, T. F. Crude Oil in a Shallow Sand and Gravel Aquifer—II. Organic Geochemistry. *Applied Geochemistry* **1993**, *8* (6), 551–567. https://doi.org/https://doi.org/10.1016/0883-2927(93)90013-7.

(43) Baedecker, M. J.; Eganhouse, R. P.; Bekins, B. A.; Delin, G. N. Loss of Volatile Hydrocarbons from an LNAPL Oil Source. *Journal of contaminant hydrology* **2011**, *126* (3–4), 140–152.

(44) Thorn, K. A.; Aiken, G. R. Biodegradation of Crude Oil into Nonvolatile Organic Acids in a Contaminated Aquifer near Bemidji, Minnesota. *Organic Geochemistry* **1998**, *29* (4), 909–931.

(45) Tuccillo, M. E.; Cozzarelli, I. M.; Herman, J. S. Iron Reduction in the Sediments of a Hydrocarbon-Contaminated Aquifer. *Applied Geochemistry* **1999**, *14* (5), 655–667. https://doi.org/https://doi.org/10.1016/S0883-2927(98)00089-4.

(46) Cozzarelli, I. M.; Bekins, B. A.; Baedecker, M. J.; Aiken, G. R.; Eganhouse, R. P.; Tuccillo, M. E. Progression of Natural Attenuation Processes at a Crude-Oil Spill Site: I. Geochemical Evolution of the Plume. *Journal of Contaminant Hydrology* **2001**, *53* (3), 369–385. https://doi.org/https://doi.org/10.1016/S0169-7722(01)00174-7.

(47) Amos, R. T.; Bekins, B. A.; Cozzarelli, I. M.; Voytek, M. A.; Kirshtein, J. D.; Jones, E. J. P.; Blowes, D. W. Evidence for Iron-mediated Anaerobic Methane Oxidation in a Crude Oil-contaminated Aquifer. *Geobiology* **2012**, *10* (6), 506–517.

(48) Amos, R. T.; Bekins, B. A.; Delin, G. N.; Cozzarelli, I. M.; Blowes, D. W.; Kirshtein, J. D. Methane Oxidation in a Crude Oil Contaminated Aquifer: Delineation of Aerobic Reactions at the Plume Fringes. *Journal of contaminant hydrology* **2011**, *125* (1–4), 13–25.

(49) Amos, R. T.; Bekins, B. A.; Cozzarellli, I. M.; Voytek, M. A.; Kirshtein, J.; Delin, G. N.; Blowes, D. W. Methane Oxidation in a Crude Oil Contaminated Aquifer. *Geochimica et Cosmochimica Acta Supplement* **2008**, *72* (12), A20.

(50) Sihota, N. J.; Singurindy, O.; Mayer, K. U. CO2-Efflux Measurements for Evaluating Source Zone Natural Attenuation Rates in a Petroleum Hydrocarbon Contaminated Aquifer. *Environmental Science & Technology* **2011**, *45* (2), 482–488.

(51) Sihota, N. J. J. Novel Approaches for Quantifying Source Zone Natural Attenuation of Fossil and Alternative Fuels. University of British Columbia 2014.

(52) Bekins, B. A.; Hostettler, F. D.; Herkelrath, W. N.; Delin, G. N.; Warren, E.; Essaid, H. I. Progression of Methanogenic Degradation of Crude Oil in the Subsurface. *Environmental Geosciences* **2005**, *12* (2), 139–152.

(53) Jakobsen, R.; Postma, D. Redox Zoning, Rates of Sulfate Reduction and Interactions with Fe-Reduction and Methanogenesis in a Shallow Sandy Aquifer, Rømø, Denmark. *Geochimica et Cosmochimica Acta* **1999**, *63* (1), 137–151.

(54) Dzombak, D. A.; Morel, F. M. M. *Surface Complexation Modeling: Hydrous Ferric Oxide*; A Wiley-Interscience publication; Wiley, 1990.

(55) Tahervand, S.; Jalali, M. Sorption and Desorption of Potentially Toxic Metals (Cd, Cu, Ni and Zn) by Soil Amended with Bentonite, Calcite and Zeolite as a Function of PH. *Journal of Geochemical Exploration* **2017**, *181*, 148–159.

(56) Guo, H.; Ben, D.; Berner, Z. Removal of Arsenic from Aqueous Solution by Natural Siderite and Hematite. *Applied Geochemistry - APPL GEOCHEM* **2007**, *22*. https://doi.org/10.1016/j.apgeochem.2007.01.004.

(57) van Cappellen, P.; Charlet, L.; Stumm, W.; Wersin, P. A Surface Complexation Model of the Carbonate Mineral-Aqueous Solution Interface. *Geochimica et Cosmochimica Acta* **1993**, *57* (15), 3505–3518. https://doi.org/https://doi.org/10.1016/0016-7037(93)90135-J.

(58) Zachara, J. M.; Cowan, C. E.; Resch, C. T. Sorption of Divalent Metals on Calcite. *Geochimica et cosmochimica acta* **1991**, *55* (6), 1549–1562.

(59) Schreiber, M. E.; Simo, J. A.; Freiberg, P. G. Stratigraphic and Geochemical Controls on Naturally Occurring Arsenic in Groundwater, Eastern Wisconsin, USA. *Hydrogeology Journal* **2000**, *8* (2), 161–176.

(60) Erickson, M. L.; Malenda, H. F.; Berquist, E. C.; Ayotte, J. D. Arsenic Concentrations after Drinking Water Well Installation: Time-Varying Effects on Arsenic Mobilization. *Science of the Total Environment* **2019**, *678*, 681–691.

(61) Erickson, M. L.; Barnes, R. J. Arsenic Concentration Variability in Public Water System Wells in Minnesota, USA. *Applied Geochemistry* **2006**, *21* (2), 305–317.

(62) Barcelona, by M.; Puls, R.; Kaminski, D. *Ground Water Purging and Sampling Methods: History vs. Hysteria*; 2005.

(63) Langmuir, D. *Aqueous Environmental Geochemistry*; 1997.

(64) Kohler, M.; Kent, D. B.; Cozzarelli, I. M.; Elzings, E.; Scheiderich, K.; Bekins, B. A. *Chemical Forms of Sediment-Bound Fe(II) in Sediments from an Aquifer Contaminated by a Petroleum Spill*; 2018.

(65) Stumm, W.; Kummert, R.; Sigg, L. A Ligand Exchange Model for the Adsorption of Inorganic and Organic Ligands at Hydrous Oxide Interfaces. *Croatica chemica acta* **1980**, *53* (2), 291–312.

(66) Davis, J. A.; Leckie, J. O. Surface Ionization and Complexation at the Oxide/Water Interface II. Surface Properties of Amorphous Iron Oxyhydroxide and Adsorption of Metal Ions. *Journal of colloid and interface science* **1978**, *67* (1), 90–107.

(67) Hiemstra, T.; van Riemsdijk, W. H. A Surface Structural Approach to Ion Adsorption: The Charge Distribution (CD) Model. *Journal of colloid and interface science* **1996**, *179* (2), 488–508.

(68) Deverel, S. J.; Fujii, R. Chemistry of Trace Elements in Soils and Ground Water. *Agricultural Salinity Assessment and Management. American Society of Civil Engineers, New York* **1990**, 64–90.

(69) Ziegler, B. A.; Ng, G. H.-C.; Cozzarelli, I. M.; Dunshee, A. J.; Schreiber, M. E. A Reactive Transport Model of Arsenic Cycling in a Petroleum-Contaminated Aquifer. *Water* **2021**, *13*.

(70) McGuire, J. T.; Cozzarelli, I. M.; Bekins, B. A.; Link, H.; Martinović-Weigelt, D. Toxicity Assessment of Groundwater Contaminated by Petroleum Hydrocarbons at a Well-Characterized, Aged, Crude Oil Release Site. *Environmental Science & Technology* **2018**, *52* (21), 12172–12178. https://doi.org/10.1021/acs.est.8b03657.